Mode conversion using stimulated Brillouin scattering in nanophotonic silicon waveguides

Iman Aryanfar,[1,*] Christian Wolff,[2] M. J. Steel,[3] Benjamin J. Eggleton[1] and Christopher G. Poulton[2]

[1]*Centre for Ultrahigh bandwidth Devices for Optical Systems (CUDOS), Institute of Photonics and Optical Science (IPOS), School of Physics, University of Sydney, Sydney, NSW 2006, Australia*

[2]*CUDOS, School of Mathematical Sciences, University of Technology, Sydney, NSW 2007, Australia*

[3]*CUDOS and MQ Photonics Research Centre, Department of Physics and Astronomy, Macquarie University, NSW 2109, Australia*

[*]*iman@physics.usyd.edu.au*

Abstract: We theoretically and numerically investigate Stimulated Brillouin Scattering generated mode conversion in high-contrast suspended silicon nanophotonic waveguides. We predict significantly enhanced mode conversion when the linked effects of radiation pressure and motion of the waveguide boundaries are taken into account. The mode conversion is more than 10 times larger than would be predicted if the effect of radiation pressure is not taken into account: we find a waveguide length of 740 μm is required for 20dB of mode conversion, assuming a total pump power of 1W. This is sufficient to bring the effect into the realm of chip-scale photonic waveguides. We explore the interaction between the different types of acoustic modes that can exist within these waveguides, and show how the presence of these modes leads to enhanced conversion between the different possible optical modes.

OCIS codes: (190.0190) Nonlinear optics; (190.2640) Stimulated scattering, modulation, etc.; (190.4360) Nonlinear optics, devices.

References and links

1. R. W. Boyd, Nonlinear Optics 3rd ed. (Academic Press, 2003).
2. M. Tomes and T. Carmon, "Photonic micro-electromechanical systems vibrating at x-band (11-GHz) rates," Phys. Rev. Lett. **102**, 113601 (2009).
3. M. S. Kang, A. Nazarkin, A. Brenn, and P. St J. Russell, "Tightly trapped acoustic phonons in photonic crystal fibres as highly nonlinear artificial Raman oscillators," Nature Phys. **5**, 276–280 (2009).
4. Y. Okawachi, M. Bigelow, J. Sharping, Z. Zhu, A. Schweinsberg, D. Gauthier, R. Boyd, and A. Gaeta, "Tunable all-Optical delays via Brillouin slow light in an optical fiber," Phys. Rev. Lett. **94**, 153902 (2005).
5. Z. Zhu, D. J. Gauthier, and R. W. Boyd, "Stored light in an optical fiber via stimulated Brillouin scattering," Science **318**, 1748–50 (2007).
6. L. F. Stokes, M. Chodorow, and H. J. Shaw, "All-fiber stimulated Brillouin ring laser with submilliwatt pump threshold," Opt. Lett. **7**, 509–11 (1982).
7. A. Byrnes, R. Pant, E. Li, D.-Y. Choi, C. G. Poulton, S. Fan, S. Madden, B. Luther-Davies, and B. J. Eggleton, "Photonic chip based tunable and reconfigurable narrowband microwave photonic filter using stimulated Brillouin scattering," Opt. Express **20**, 18836–45 (2012).

#221374 - $15.00 USD Received 26 Aug 2014; revised 17 Oct 2014; accepted 7 Nov 2014; published 14 Nov 2014

8. D. Braje, L. Hollberg, and S. Diddams, "Brillouin-enhanced hyperparametric generation of an optical frequency comb in a monolithic highly nonlinear fiber cavity pumped by a cw laser," Phys. Rev. Lett. **102**, 193902 (2009).
9. T. F. S. Büttner, I. V. Kabakova, D. D. Hudson, R. Pant, C. G. Poulton, A. C. Judge, and B. J. Eggleton, "Phase-locking and pulse generation in multi-frequency Brillouin oscillator via four wave mixing," Sci. Rep. **4**, 5032 (2014).
10. X. Huang and S. Fan, "Complete all-optical silica fiber isolator via stimulated Brillouin scattering," J. Lightw. Tech. **29**, 2267–2275 (2011).
11. Z. Yu and S. Fan, "Optical isolation based on nonreciprocal phase shift induced by interband photonic transitions," Appl. Phys. Lett. **94**, 171116 (2009).
12. M. S. Kang, A. Brenn, and P. St J. Russell, "All-optical control of gigahertz acoustic resonances by forward stimulated interpolarization scattering in a photonic crystal fiber," Phys. Rev. Lett. **105**, 153901 (2010).
13. M. S. Kang, A. Butsch, and P. St J. Russell, "Reconfigurable light-driven opto-acoustic isolators in photonic crystal fibre," Nature Photon. **5**, 549–553 (2011).
14. C. G. Poulton, R. Pant, A. Byrnes, S. Fan, M. J. Steel, and B. J. Eggleton, "Design for broadband on-chip isolator using Stimulated Brillouin Scattering in dispersion-engineered chalcogenide waveguides," Opt. Express **20**, 21235–21246 (2012).
15. M.-C. Tien, T. Mizumoto, P. Pintus, H. Kromer, and J. E. Bowers, "Silicon ring isolators with bonded nonreciprocal magneto-optic garnets," Opt. Express **19**, 11740–5 (2011).
16. J. Fujita, M. Levy, R. M. Osgood Jr, L. Wilkens, and H. Dotsch, "Waveguide optical isolator based on Mach-Zehnder interferometer," Appl. Phys. Lett. **76**, 2158 (2000).
17. B. J. H. Stadler and T. Mizumoto, "Integrated magneto-optical materials and isolators: a review," IEEE Photonics Journal **6**, 1–15 (2014).
18. B. J. Eggleton, C. G. Poulton, and R. Pant, "Inducing and harnessing stimulated Brillouin scattering in photonic integrated circuits," Advances in Optics and Photonics **5**, 536–587 (2013).
19. P. T. Rakich, P. Davids, and Z. Wang, "Tailoring optical forces in waveguides through radiation pressure and electrostrictive forces," Opt. Express **18**, 14439–53 (2010).
20. P. T. Rakich, Z. Wang, and P. Davids, "Scaling of optical forces in dielectric waveguides: rigorous connection between radiation pressure and dispersion," Opt. Lett. **36**, 217–9 (2011).
21. H. Shin, W. Qiu, R. Jarecki, J. A. Cox, R. H. Olsson, A. Starbuck, Z. Wang, and P. T. Rakich, "Tailorable stimulated Brillouin scattering in nanoscale silicon waveguides," Nature Commun. **4**, 1944 (2013).
22. H. Lira, Z. Yu, S. Fan, and M. Lipson, "Electrically driven nonreciprocity induced by interband photonic transition on a silicon chip," Phys. Rev. Lett. **109**, 033901 (2012).
23. D.-W. Wang, H.-T. Zhou, M.-J. Guo, J.-X. Zhang, J. Evers, and S.-Y. Zhu, "Optical diode made from a moving photonic crystal," Phys. Rev. Lett. **110**, 093901 (2013).
24. W. Qiu, P. T. Rakich, H. Shin, H. Dong, M. Soljacic, and Z. Wang, "Stimulated Brillouin scattering in nanoscale silicon step-index waveguides : a general framework of selection rules and calculating SBS gain," Opt. Express **21**, 276–280 (2013).
25. C. Wolff, M. J. Steel, B. J. Eggleton, and C. G. Poulton, "Stimulated Brillouin scattering in integrated photonic waveguides: forces, scattering mechanisms and coupled mode analysis," arXiv:1407.3521 pp. 1–17 (2014).
26. A. M. Vengsarkar, P. J. Lemaire, J. B. Judkins, V. Bhatia, T. Erdogan, and J. E. Sipe, "Long-period fiber gratings as band-rejection filters," J. Lightw. Tech. **14**, 58–65 (1996).
27. P. T. Rakich, C. Reinke, R. Camacho, P. Davids, and Z. Wang, "Giant enhancement of stimulated Brillouin scattering in the subwavelength limit," Phys. Rev. X **2**, 011008 (2012).
28. K. David, "Photoelastic tensor of silicon and the volume dependence of the average gap," Phys. Rev. Lett. **32**, 1196–1199 (1974).
29. R. Pant, C. G. Poulton, D.-Y. Choi, H. Mcfarlane, S. Hile, E. Li, L. Thevenaz, B. Luther-Davies, S. J. Madden, and B. J. Eggleton, "On-chip stimulated Brillouin scattering," Opt. Express **19**, 8285–90 (2011).
30. L. Yin and G. P. Agrawal, "Impact of two-photon absorption on self-phase modulation in silicon waveguides," Opt. Lett. **32**, 2031 (2007).
31. H. K. Tsang, C. S. Wong, T. K. Liang, I. E. Day, S. W. Roberts, A. Harpin, J. Drake, and M. Asghari, "Optical dispersion, two-photon absorption and self-phase modulation in silicon waveguides at 1.5μm wavelength," Appl. Phys. Lett. **80**, 416 (2002).
32. R. Jones, H. Rong, A. Liu, A. W. Fang, M. Paniccia, D. Hak, and O. Cohen, "Net continuous wave optical gain in a low loss silicon-on-insulator waveguide by stimulated Raman scattering," Opt. Express **13**, 519–525 (2005).

1. Introduction

Stimulated Brillouin Scattering (SBS) is a strong nonlinear interaction between the electromagnetic and mechanical waves in an optical waveguide [1]. In the past decade SBS has been demonstrated in a number of different applications in photonics, such as signal processing [2,3], slow [4] and stored light [5], Brillouin lasers [6], microwave photonics [7] and frequency comb

#221374 - $15.00 USD Received 26 Aug 2014; revised 17 Oct 2014; accepted 7 Nov 2014; published 14 Nov 2014

generation [3, 8, 9]. An interesting and potentially important use for the SBS interaction is to drive transitions between modes in multimode waveguides [10]. Although mode conversion using gratings or other structures such as Mach-Zehnder interferometers [11] is well-established, SBS-based mode conversion is non-reciprocal, in the sense that the effect is induced in the direction co-propagating with a pump beam but not in the counter-propagating direction [12]. This makes SBS-based mode conversion important for optical applications such as optical isolation [10, 13, 14]. SBS-based mode converters may be also simpler to fabricate and more flexible in application than non-reciprocal structures that use Faraday rotation from embedded magneto-optic elements [15–17].

For practical applications, the SBS interaction is usually thought to require very long waveguide lengths, because of the low SBS gain that is characteristic of the low-index-contrast fibres commonly used in photonics. Recently however, two new approaches have been suggested for achieving high SBS gain, potentially enabling SBS-based mode-conversion in the very short waveguides that occur on optical chips. The first involves the use of materials that possess a high refractive index n (SBS gain scales as n^8), while simultaneously confining the acoustic mode in order to achieve good overlap with the optical field. This strategy has been demonstrated in a number of recent experiments [18]. The second approach is to make use of the effect of radiation pressure, which is dramatically enhanced for high-contrast waveguides with small cross-sections [19–21]. The acoustic modes in SBS are generated by optical forces arising from the pump, and for small waveguides the forces arising from radiation pressure at the waveguide boundary can be at least as large as the forces from electrostriction throughout the waveguide. These two effects can also reinforce, leading to large SBS gain. Recent experiments have demonstrated forward SBS scattering in silicon, which has a very small electrostrictive constant [21].

Earlier studies have also demonstrated mode conversion in nanophotonic devices, either using magneto-optical activity [15–17] or time-dependent modulation of the material properties [22, 23]. SBS-based mode conversion has also been studied in photonic crystal fibers [12, 13]. It is important to note however that the proposed SBS-based devices require long lengths (15 m) of waveguide for conversion to occur, and that the use of a single pump in the configuration limited the bandwidth of the device to that of the SBS linewidth. In addition, the dominant driving mechanism in these fiber devices was electrostriction/photoelasticity: the effects of radiation pressure/boundary motion were able to be neglected. An investigation that takes into account both electrostriction and radiation pressure, using a broadband configuration in which the pumps induce the acoustic wave that drives the mode transition [10], is necessary for the successful implementation of these devices in silicon and other high index-contrast platforms.

In this paper, we theoretically and numerically investigate SBS-based mode conversion for small, high contrast, suspended crystalline silicon waveguides, considering both radiation pressure and electrostriction. We find significant enhancement of SBS-based mode conversion in these waveguides when radiation pressure is taken into account. This enhancement is driven by two phenomena. Firstly, radiation pressure leads to enhanced SBS gain, as has been shown theoretically in [24]. Secondly, radiation pressure is inextricably linked with scattering from the motion of the waveguide boundaries [25]. This scattering takes place in addition to the photoelastic effect normally associated with SBS, and can in principle produce stronger acoustic vibrations along the waveguide, which scatter light from one mode to another in the manner of a long-period grating [26]. A central aim of this work is to extend previous work on SBS gain enhancement [24, 27], by investigating the main effects of these additional processes on mode conversion. We also explore the effect of waveguide geometry on the mode conversion process. We find that there exist classes of mode conversion—for example, between differently-polarized optical modes—that do not appear in the conventional scalar SBS theory.

#221374 - $15.00 USD Received 26 Aug 2014; revised 17 Oct 2014; accepted 7 Nov 2014; published 14 Nov 2014

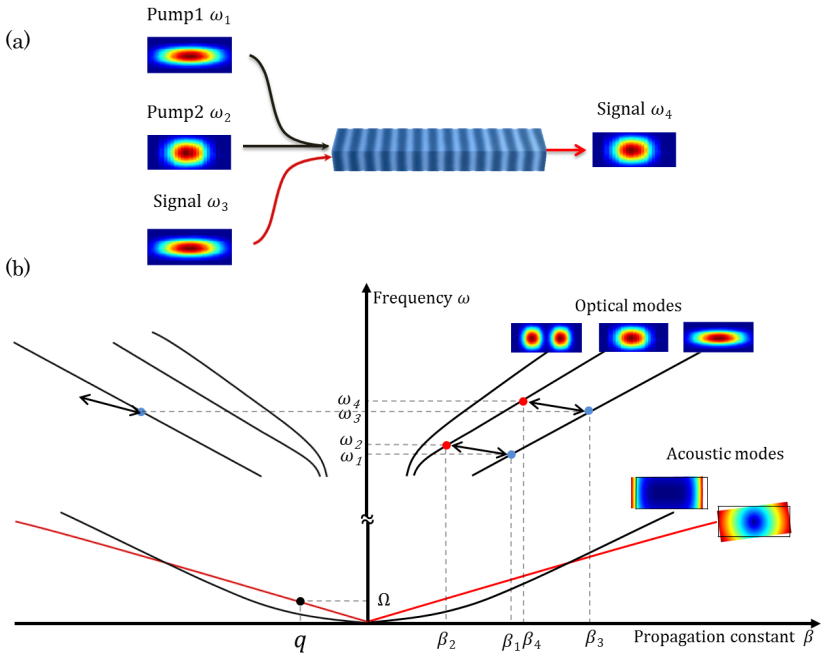

Fig. 1. a) Schematic of mode conversion operation. Two differently polarized fundamental modes are pumped into a suspended high contrast waveguide to excite a guided acoustic mode. The acoustic mode creates a temporary traveling grating which drives conversion from the signal in the *x*-polarized fundamental mode at ω_3 to a *y*-polarized fundamental mode at frequency ω_4. b) A simplified dispersion diagram illustrating the photonic conversion process with respect to optical and acoustic modes. The black dot indicates the acoustic mode at frequency $\Omega = \omega^{(2)} - \omega^{(1)}$ which is able to phase match between the two optical modes, so having propagation constant $q = \beta^{(2)} - \beta^{(1)}$. An optical signal which is traveling in counterpropagating direction does not satisfy the phase matching condition.

These interactions involve hybrid acoustic modes, such as quasi-flexural and quasi-torsional modes, which become important in small suspended waveguides and which induce waveguide boundary motions that scatter the optical field strongly. We examine the classes of acoustic modes that lead to mode conversion between the different classes of optical modes, and investigate how the mode conversion depends on the presence or absence of the radiation pressure (and concomitant boundary motion) effect. Finally, we explore the parameter space for high index-contrast waveguides, and explain the underlying physics of the mode conversion process in these waveguides.

2. Principle of operation and theory

In the following we consider interaction between modes in a suspended rectangular waveguide. The principle for achieving mode conversion via SBS is as follows [10]: two CW optical pumps at frequencies $\omega^{(1)}$ and $\omega^{(2)}$ are launched into a waveguide in such a way that they excite two different optical modes – these can be two modes of differing polarization, or, depending on the size of the waveguide, they can be the fundamental and a higher order mode. The interaction between these two pumps generates an acoustic field in the system at the beat frequency $\Omega = \omega^{(2)} - \omega^{(1)}$ with propagation constant $q = \beta^{(2)} - \beta^{(1)}$ via contributions from electrostriction and radiation pressure [19, 27]. These conditions arise from the necessary con-

#221374 - $15.00 USD Received 26 Aug 2014; revised 17 Oct 2014; accepted 7 Nov 2014; published 14 Nov 2014

servation of energy and momentum when a pump photon is converted into a Stokes photon and a phonon (see Fig. 1(b)). If the pair (q,Ω) lies on an acoustic dispersion curve then the acoustic mode may be resonantly excited by the optical modes subject to appropriate symmetry conditions [24]. Consequently, the acoustic mode induces a traveling grating, both via the density fluctuations in the acoustic mode, as well as via direct motion of the waveguide boundaries. This grating drives transitions between the same two optical modes as the pump, but over a wide wavelength range: a signal having the same mode as pump 1 at frequency $\omega^{(3)}$ will interact with the traveling photo-elastic grating to form a second signal with frequency $\omega^{(4)} = \omega^{(3)} + \Omega$ and mode character the same as pump 2. This process is illustrated in Fig. 1(a): here two differently polarized fundamental modes interact to drive mode conversion. Figure 1(b) depicts the phase matching that is necessary for this process to occur. In this investigation we assume that it is possible to couple only two optical modes, and so only four waves take part in the interaction. In principle it is possible to generate higher-order SBS lines at different frequencies, particularly when the acoustic wavenumber is small [3]. We neglect such higher-order effects here.

The mode conversion process depends on the interaction between optical and acoustic fields over the length of the waveguide. This interaction can be modeled using coupled-mode theory. A number of such descriptions exist. We follow the approach of our recent formulation in [25]. We consider four optical fields, consisting of two pumps and two signals, and a single acoustic field. Each optical mode has a transverse electric field $\mathbf{E}^{(j)}$, that can be written as

$$\mathbf{E}^{(i)}(x,y,z,t) = a^{(i)}(z,t)\,\widetilde{\mathbf{e}}^{(i)}(x,y)\,\exp\Big(\,\mathrm{i}\beta^{(i)}z - \,\mathrm{i}\omega^{(i)}t\Big) \;+\; \text{c.c.}\,, \tag{1}$$

where $\widetilde{\mathbf{e}}^{(i)}(x,y)$ is the transverse profile of the i^{th} mode, $a^{(i)}(z,t)$ is its slowly varying mode amplitude and the index $i \in \{1,2,3,4\}$ labels the individual optical modes. For simplicity, we assume that the field distributions of the pump and signal waves in the same modes are identical:

$$\widetilde{\mathbf{e}}^{(3)} = \widetilde{\mathbf{e}}^{(1)}, \qquad \widetilde{\mathbf{e}}^{(4)} = \widetilde{\mathbf{e}}^{(2)}. \tag{2}$$

As the typical frequency separation might be only a few THz, this is normally a very good approximation. Analogously, the acoustic wave that is the result of the interaction between the two optical pumps can be written as

$$\mathbf{U}(x,y,z,t) = b(z,t)\,\widetilde{\mathbf{u}}(x,y)\,\exp(\,\mathrm{i}qz - \,\mathrm{i}\Omega t) \;+\; \text{c.c.}, \tag{3}$$

where $b(z,t)$ is the acoustic mode amplitude and $\widetilde{\mathbf{u}}(x,y)$ is the displacement of the acoustic mode over the waveguide cross-section. For normalization purposes, we need the total power carried by each of these modes:

$$\mathscr{P}_1 = \mathscr{P}_3 = 2\int \mathrm{d}^2 r\;\hat{\mathbf{z}}\cdot([\widetilde{\mathbf{e}}^{(1)}]^*\times\widetilde{\mathbf{h}}^{(1)}), \qquad \mathscr{P}_2 = \mathscr{P}_4 = 2\int \mathrm{d}^2 r\;\hat{\mathbf{z}}\cdot([\widetilde{\mathbf{e}}^{(2)}]^*\times\widetilde{\mathbf{h}}^{(2)}), \tag{4}$$

$$\mathscr{P}_b = 2\,\mathrm{i}\Omega\int \mathrm{d}^2 r\;\sum_{ikl} c_{zikl}u_i^*\partial_k u_l, \tag{5}$$

where $\hat{\mathbf{z}}$ is the unit vector along the waveguide, $\widetilde{\mathbf{h}}^{(i)}$ is the magnetic field complex amplitude of the i^{th} optical mode and c is the stiffness tensor of the waveguide's material. The coupled amplitude equations for the optical pump sources and signals are as follows [25]:

$$\partial_z a^{(1)} = \frac{\mathrm{i}\omega^{(1)}Q_1}{\mathscr{P}_1}a^{(2)}b^*, \qquad \partial_z a^{(2)} = \frac{\mathrm{i}\omega^{(2)}Q_2}{\mathscr{P}_2}a^{(1)}b, \tag{6}$$

$$\partial_z a^{(3)} = \frac{\mathrm{i}\omega^{(3)}Q_3}{\mathscr{P}_3}a^{(4)}b^*, \qquad \partial_z a^{(4)} = \frac{\mathrm{i}\omega^{(4)}Q_4}{\mathscr{P}_4}a^{(3)}b. \tag{7}$$

#221374 - $15.00 USD Received 26 Aug 2014; revised 17 Oct 2014; accepted 7 Nov 2014; published 14 Nov 2014

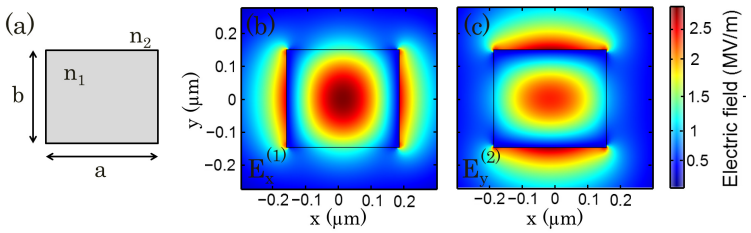

Fig. 2. a) Waveguide geometry, silicon suspended in air with a rectangular cross-section of $a = 350$ nm by $b = 300$ nm. b) x-polarized mode 1 and c) y-polarized mode 2, as the two optical pumps.

Here, ∂_z denotes the partial derivative along the waveguide. We apply a long-waveguide approximation for the acoustic envelope b:

$$b = \frac{\mathrm{i}\Omega Q_b}{\mathscr{P}_b \alpha}[a^{(1)}]^* a^{(2)}, \tag{8}$$

where $\alpha = \Gamma_B / v_b$ is the phonon power loss (in units of m^{-1}), related to the phonon lifetime τ by $\alpha = 1/(v_b \tau)$

and related to the Brillouin line width Γ_B (38GHz in the case of silicon) via the acoustic group velocity v_b. For simplicity, we consider the acoustic Q-factor to be 1000 in this calculation [21]. Due to energy conservation [25] and the fact that the pump and signal modes are taken identical, all optical and mechanical coupling constants Q_i are identical up to complex conjugation. Their value is the overlap integral between the optical force density $\widetilde{\mathbf{f}}$ and the displacement field of the acoustic mode:

$$Q_1 = Q_2^* = Q_3 = Q_4^* = Q_b = \int \widetilde{\mathbf{u}}^* \cdot \widetilde{\mathbf{f}} \; \mathrm{d}x \, \mathrm{d}y, \tag{9}$$

where the optical force field comprises contributions from pure body forces and boundary pressure terms: $\widetilde{\mathbf{f}} = \widetilde{\mathbf{f}}^{(\mathrm{body})} + \widetilde{\mathbf{f}}^{(\mathrm{boundary})}$. The derivation of the body forces, boundary pressure and Q_1, Q_2, etc. can be found in [25]. For the former, we assume the divergence

$$\widetilde{f}_i^{(\mathrm{body})} = \sum_j \partial_j \widetilde{\sigma}_{ij}^{(\mathrm{es})} \tag{10}$$

of the phase-matched part of the electrostrictive stress tensor, which in turn can be conveniently expressed in Voigt notation:

$$\begin{bmatrix} \widetilde{\sigma}_{xx}^{(\mathrm{es})} \\ \widetilde{\sigma}_{yy}^{(\mathrm{es})} \\ \widetilde{\sigma}_{zz}^{(\mathrm{es})} \\ \widetilde{\sigma}_{yz}^{(\mathrm{es})} \\ \widetilde{\sigma}_{xz}^{(\mathrm{es})} \\ \widetilde{\sigma}_{xy}^{(\mathrm{es})} \end{bmatrix} = -\varepsilon_0 \varepsilon_r^2 \begin{bmatrix} p_{11} & p_{12} & p_{13} & 0 & 0 & 0 \\ p_{21} & p_{22} & p_{23} & 0 & 0 & 0 \\ p_{31} & p_{32} & p_{33} & 0 & 0 & 0 \\ 0 & 0 & 0 & p_{44} & 0 & 0 \\ 0 & 0 & 0 & 0 & p_{55} & 0 \\ 0 & 0 & 0 & 0 & 0 & p_{66} \end{bmatrix} \begin{bmatrix} [\widetilde{e}_x^{(1)}]^* \widetilde{e}_x^{(2)} \\ [\widetilde{e}_y^{(1)}]^* \widetilde{e}_y^{(2)} \\ [\widetilde{e}_z^{(1)}]^* \widetilde{e}_z^{(2)} \\ [\widetilde{e}_y^{(1)}]^* \widetilde{e}_z^{(2)} + [\widetilde{e}_z^{(1)}]^* \widetilde{e}_y^{(2)} \\ [\widetilde{e}_x^{(1)}]^* \widetilde{e}_z^{(2)} + [\widetilde{e}_z^{(1)}]^* \widetilde{e}_x^{(2)} \\ [\widetilde{e}_x^{(1)}]^* \widetilde{e}_y^{(2)} + [\widetilde{e}_y^{(1)}]^* \widetilde{e}_x^{(2)} \end{bmatrix}. \tag{11}$$

Analogously, the boundary force generated by radiation pressure is computed from $\widetilde{f}_i^{(\mathrm{rp})} = \sum_j \partial_j \widetilde{\sigma}_{ij}^{(\mathrm{rp})}$ where $\widetilde{\sigma}_{ij}^{(\mathrm{rp})}$ is the phase-matched component of the Maxwell stress tensor:

$$\widetilde{\sigma}_{ij}^{(\mathrm{rp})} = \varepsilon_0 \varepsilon_r [\widetilde{e}_i^{(1)}]^* \widetilde{e}_j^{(2)} + \mu_0 [\widetilde{h}_i^{(1)}]^* \widetilde{h}_j^{(2)} - \frac{1}{2} \delta_{ij} \left(\varepsilon_0 \varepsilon_r [\widetilde{\mathbf{e}}^{(1)}]^* \cdot \widetilde{\mathbf{e}}^{(2)} + \mu_0 [\widetilde{\mathbf{h}}^{(1)}]^* \cdot \widetilde{\mathbf{h}}^{(2)} \right), \tag{12}$$

#221374 - $15.00 USD Received 26 Aug 2014; revised 17 Oct 2014; accepted 7 Nov 2014; published 14 Nov 2014

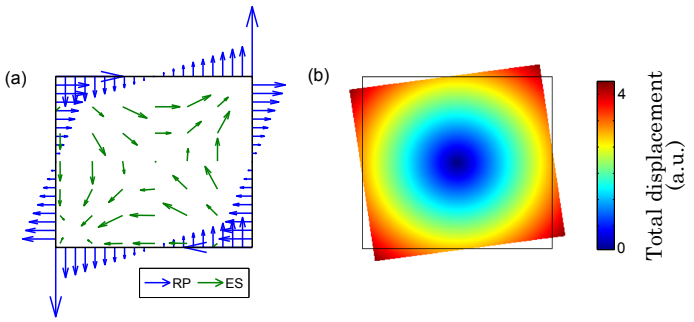

Fig. 3. a) Force distribution of radiation pressure (blue) and electrostriction body force (green) generated by applying two differently polarized optical modes, b) corresponding magnitude of the total displacement of the torsional acoustic mode excited by the forces. The strength of the acoustic oscillation is grossly exaggerated.

where μ_0 is the magnetic permittivity of free space, ε_r is the relative electric permittivity, and δ_{ij} is the Kronecker delta. From these expressions, the SBS gain in the waveguide (in units of $\mathrm{m}^{-1}\mathrm{W}^{-1}$) is given by [25]

$$G_{\,(\mathrm{SBS})} = \frac{2\omega^{(1)}\Omega|Q_1|^2}{\mathscr{P}_1\mathscr{P}_2\mathscr{P}_b\alpha}. \tag{13}$$

This expression provides the basis for comparison of mode conversion efficiency under various conditions in the following.

3. Mode conversion in a suspended silicon waveguide

In this section we investigate the process of mode conversion in a high contrast material, using a suspended silicon waveguide as a specific example. We first consider the geometry shown in Fig. 2(a), that is, a suspended silicon waveguide with a rectangular cross-section of 350×300 nm. We assume isotropic mechanical and electromagnetic properties for silicon, with Young's modulus $E = 170\times10^9$ Pa, Poisson's ratio $\nu = 0.28$, density $\rho = 2329\ \mathrm{kg/m}^3$, and refractive index $n = 3.5$ [27]. The photoelastic coefficients of silicon have been reported to be $p_{11} = -0.09$, $p_{12} = +0.017$, $p_{44} = -0.054$, $p_{11} = p_{22} = p_{33}$, $p_{12} = p_{21} = p_{13} = p_{31}$ and $p_{44} = p_{55} = p_{66}$ [28].

We first consider mode conversion between two cross polarized optical modes. To compute all optical and acoustic fields in this structure we use the commercial finite element software COMSOL. The computational domain for the optical modes is defined as a square of $3\ \mu\mathrm{m}\times3\ \mu\mathrm{m}$, with perfectly conducting electric boundary conditions defined on the edge of the domain, and with a maximum mesh size of 60 nm. Figures 2(b) and (c) illustrate two differently polarized electric fields taken as the two optical pumps. The optical forces due to these two differently polarized optical pumps were calculated by Eqs. (10-12) and are shown in Fig. 3(a). The green and blue arrows indicate the force distribution for the electrostriction body force and for the radiation pressure respectively. It can be seen that the overall force distribution results in a shear strain of the waveguide structure.

The calculated acoustic dispersion curves of this structure are shown in Fig. 4. This information is needed in order to determine which acoustic modes are phase matched to the optical fields. In addition, each acoustic mode possesses a different symmetry so that it may or may not be excited by the optical force distribution. The appropriate symmetry for coupling to the force distribution shown in Fig. 3(a) is a torsional-type mode, see Fig. 3(b): flexural and longitudinal modes are only marginally excited. The torsional-type mode is indicated by the red line shown

#221374 - $15.00 USD Received 26 Aug 2014; revised 17 Oct 2014; accepted 7 Nov 2014; published 14 Nov 2014

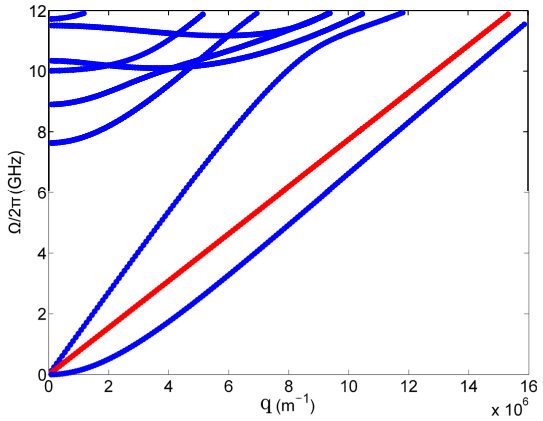

Fig. 4. Calculated acoustic dispersion curves for the 350×300 nm suspended silicon waveguide. The red line corresponds to interaction between differently polarized optical pumps that excites quasi-torsional acoustic mode redwhich is phase-matched based on the beat between the two optical modes at the beat frequency $\Omega = \omega^{(2)} - \omega^{(1)}$ with propagation constant $q = \beta^{(2)} - \beta^{(1)}$.

in Fig. 4; in an experiment this mode would be brought into resonance by adjusting the frequency spacing between the two optical pumps. Given the difference in propagation constant between the two (differently-polarized) pumps in this particular waveguide, the acoustic mode must have a propagation constant $q = 9.7 \times 10^5$ m^{-1}, which leads (from Fig. 4) to an acoustic frequency $\Omega/2\pi = 750$ MHz. The SBS gain calculated by Eq. (13) is 1.65×10^4 m^{-1}W^{-1}, which is high relative to the gain in both fibers and on-chip devices [29], since both forces due to electrostriction and radiation pressure induced on the boundary have the correct symmetry.

The acoustic field generated by two optical pumps drives mode conversion between the *x*- and *y*-polarized optical modes at different frequencies. To qualitatively characterize the amount of conversion that occurs over a given waveguide length, we integrate the coupled mode equations Eq. (7) and (8) along the waveguide to see the evolution of all optical and acoustic fields. We first consider the situation where the electrostriction body force co-exists with radiation pressure, leading to a transition driven by the photoelastic effect and waveguide-boundary motion. Figure 5(a) illustrates the results of conversion for a total pump power of 1 W, which is close to the maximum likely power that the waveguide can support without damage. Here we can see that almost all the power from signal mode 1 (shown by the red solid line) is transferred to signal mode 2 (blue solid line). The mode conversion in dB is given by

$$I_{(dB)} = 10 \log_{10} \left(\frac{P_3(z = z_{max})}{P_3(z = 0)} \right) , \tag{14}$$

where z_{max} is the length of the waveguide and $P_i = |a^{(i)}|^2 \mathscr{P}_i$ is the power carried by the i^{th} mode. For this configuration we find that the length of waveguide needed for 20 dB mode conversion can be calculated from Eq. (14), and is equal to 740 μm.

Figure 5(b) shows mode conversion for the same waveguide and input pumps, but considering SBS due to electrostriction only—that is, the effects of radiation pressure and waveguide boundary motion are neglected. It can be seen that a 20 dB signal conversion requires a much longer length of 7.4 mm, or 10 times longer than when radiation pressure effects are taken into account. This is partly due to the increased SBS gain due to radiation pressure: the gain in the electrostriction-only case is 1.66×10^3 m^{-1}W^{-1}, or ~ 10 times smaller than in the case

#221374 - $15.00 USD Received 26 Aug 2014; revised 17 Oct 2014; accepted 7 Nov 2014; published 14 Nov 2014

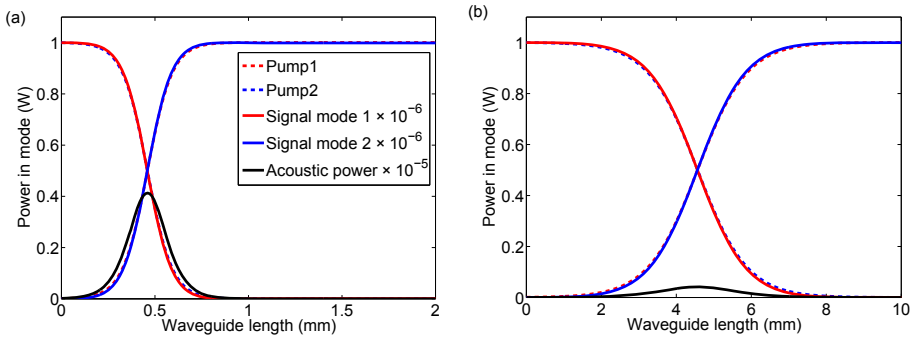

Fig. 5. Evolution of pump powers in the waveguide and corresponding photonic conversion: a) by considering both electrostriction and radiation pressure and b) considering the electrostrictive body force only. The red and blue dashed lines show the evolution of the two optical pumps in the waveguide; the red and blue solid lines show conversion between the signals. The interaction of the two pumps excites an acoustic mode, shown here by the black straight line indicating the power in the acoustic field. The initial power in the pumps was 1 mW (pump 1) and 1 W (pump 2). Note that the horizontal scale is different between the two plots.

when the radiation pressure is taken into account. The gain in the case where we just consider the radiation pressure only is 7.7×10^3 $\mathrm{m}^{-1}\mathrm{W}^{-1}$ or ~ 5 times larger than in the case when electrostriction-only is considered.

We discuss next the effects of other nonlinearities, and especially of nonlinear losses. Silicon has large nonlinear absorption, including two-photon absorption (TPA) which generates free carriers. Free carriers lead to free-carrier absorption (FCA) as well as free-carrier dispersion (FCD) [30]. The optical loss due to TPA can be calculated by $\alpha_{\mathrm{TPA}} = \beta_{\mathrm{TPA}} \dfrac{P_0}{A_{\mathrm{eff}}}$ where, $\beta_{\mathrm{TPA}} \approx 5 \times 10^{-12}$ m/W [31] which results in $\alpha_{\mathrm{TPA}} = 22\ \mathrm{m}^{-1}$ with an initial pump power of $P_0 = 1$W and $A_{\mathrm{eff}} = 0.22\ \mu\mathrm{m}^2$. This level of loss will reduce the total pump power by 2% over a 1 mm length of the waveguide and so this can be neglected. However, as TPA generates free carriers, this may have a significant effect via FCA – for CW signals and for optical pulses that are longer than the carrier lifetime, the effect of FCA can be significant even if the TPA is small, because the number of carriers can build up in the material. The TPA–induced free-carrier density $N_c = 3.7 \times 10^{24}\ \mathrm{m}^{-3}$ can be calculated from

$$N_c = \frac{\tau \beta_{\mathrm{TPA}}}{2h f_0} \left(\frac{P_0}{A_{\mathrm{eff}}} \right)^2 , \tag{15}$$

where $\tau = 10$ ns the carrier lifetime in silicon and h is Planck's constant. The corresponding power decay parameter is $\alpha_{\mathrm{FCA}} = \sigma N_c = 5.4 \times 10^3\ \mathrm{m}^{-1}$, where we have used $\sigma = 1.45 \times 10^{-21}\ \mathrm{m}^2$ as the scattering cross section of the carriers. For high pump powers, this level of loss would result in 99% of the total pump power being lost over a 1 mm length of the waveguide if the carriers are not removed, and is therefore a serious issue. Mechanisms for sweeping out free carriers using semiconductor junctions and an applied electric field have been demonstrated as feasible in [32], if the simpler strategy of using lower pump powers (and therefore longer waveguides) is not acceptable.

It is also known that the Kerr nonlinearity can interact in a complicated manner with SBS [9]. This interaction occurs in the presence of an optical cavity, which gives rise to counter-propagating waves that can undergo four-wave mixing (FWM) with the forward-propagating

#221374 - $15.00 USD Received 26 Aug 2014; revised 17 Oct 2014; accepted 7 Nov 2014; published 14 Nov 2014

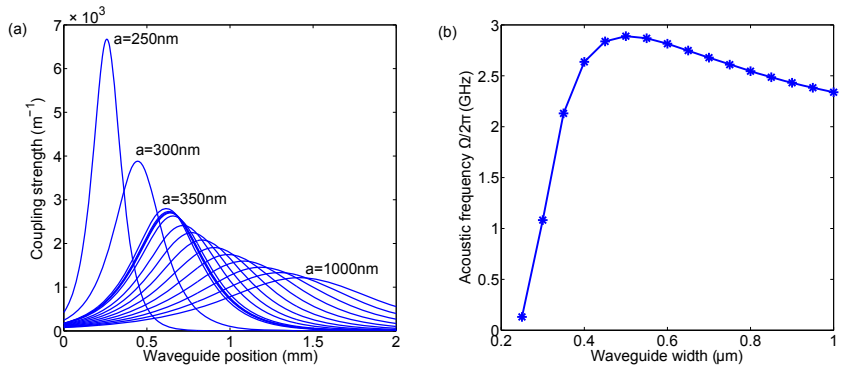

Fig. 6. a) Computed κ as a function of waveguide width ranging from 250 nm to 1000 nm over the length of 2 mm waveguide. Height of the waveguide is fixed to $b = 220$ nm. In this computation radiation pressure and electrostriction are considered. b) Frequencies of excited acoustic mode as a function of waveguide width.

pump and signals. In the situation under investigation here there is no cavity, and so such interaction is not properly phase-matched. We therefore neglect such multi-wave interactions in this analysis. The main effect of the Kerr nonlinearity will be to modulate the phase across the waveguide. The change in phase over a silicon waveguide of length 1 mm carrying 1 W of power can be computed to be $\Delta\phi = \gamma P_0 L = 0.05$ radians, with $\gamma = 53\,\mathrm{m}^{-1}\mathrm{W}^{-1}$. This is sufficiently small that it can be neglected in our calculations.

4. Exploration of parameters and different waveguides

The mechanism that drives the mode transition is that the acoustic mode sets up a traveling grating along the length of the waveguide. This grating scatters light from mode 1 into mode 2, for which it serves both as a carrier of excess energy (via the acoustic mode frequency) and momentum (via the acoustic propagation constant). This grating consists both of a dynamic modulation of the refractive index, which occurs via the photoelastic effect, and direct physical motion of the waveguide boundaries. The grating strength can be described by a z-dependent grating coupling coefficient $\kappa(z)$ (with units of m^{-1}), which is given by

$$\kappa(z) = |b(z)Q_3|\sqrt{\frac{\omega^{(3)}\omega^{(4)}}{\mathscr{P}_3\mathscr{P}_4}}. \tag{16}$$

In Fig. 6(a) we show the grating strength $\kappa(z)$, as computed from Eq. (16) for waveguide widths ranging from 250 nm to 1000 nm over a total waveguide length of 2 mm. The height of the waveguide is fixed to $b = 220$ nm. As in the previous computations, we have set the wavelength of one pump to $\lambda = 1.55\,\mu$m, which results in acoustic frequencies shown in Fig. 6(b) for the different waveguide widths. Initial pump powers are chosen as 1 mW and 1 W for pump 1 and 2 respectively. For each waveguide width, we can see that the strength of the grating $\kappa(z)$ has a peak that corresponds to the maximum acoustic intensity. We also see that due to the simple two-mode coupling between the pumps, $\kappa(z)$ obeys a scaling law that preserves the total area under the curve.

It is useful to represent the overall strength of the grating by a single quantity: this gives an idea of the length required to obtain a given transfer of power from one mode to the other, and how the grating strength depends on geometrical parameters. Given the fixed area $\int_0^L \kappa(z)\,\mathrm{d}z$, a reasonable characterization of the overall strength of the grating is the maximum obtained

#221374 - $15.00 USD Received 26 Aug 2014; revised 17 Oct 2014; accepted 7 Nov 2014; published 14 Nov 2014

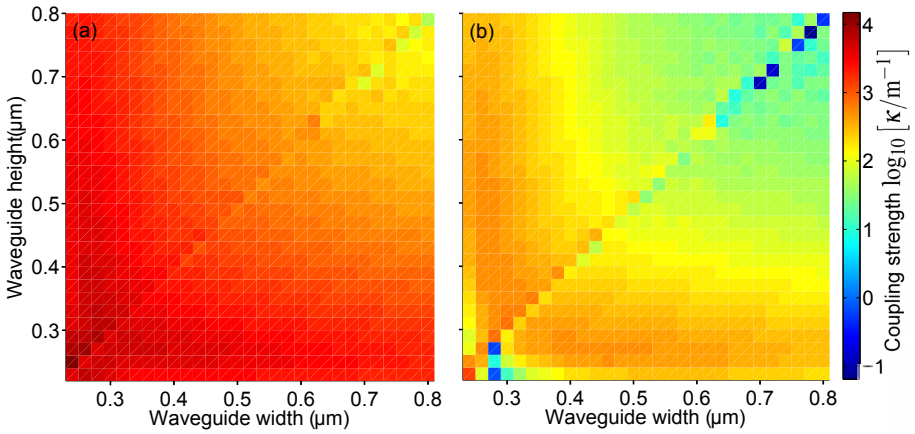

Fig. 7. Coupling strength $\kappa_{\max}$, expressed as $\log_{10}\left[\kappa/\mathrm{m}^{-1}\right]$ resulting from coupling between two differently polarized fundamental modes: a) by considering both electrostriction and radiation pressure (together with the photoelastic effect and waveguide boundary motion) and b) considering the electrostrictive effect and photoelasticity only.

value of κ for the given input pump powers. The maximum value of κ occurs always where the two input optical pumps have the same value: at this point there is an equal exchange of energy between the two pumps and the acoustic field is at its largest (see Fig. 5).

In Fig. 7 we explore how $\kappa_{\max}$ depends on the waveguide geometry. We first consider coupling between two cross polarized optical modes for varying waveguide widths and heights, starting from 230 nm and 220 nm respectively. The increment of waveguide widths and heights is equal to 20 nm, and we consider a 10 nm offset between the waveguide width and height to avoid degeneracy. Figure 7(a) shows $\kappa_{\max}$, considering both electrostriction (photoelasticity) and radiation pressure (waveguide boundary motion). Comparing the two figures it is apparent that the inclusion of the radiation pressure effects markedly increases the coupling strength. In both cases the coupling strength increases for smaller waveguide geometries—this is to be expected because the optical intensity becomes larger. The coupling reaches a maximum for the electrostrictive effect for dimensions of around 230 nm beyond which point the electromagnetic field begins to spill out of the waveguide into the surrounding volume. We also observe symmetry of the coupling about the line of equal height and width. This arises because in coupling from an *x*- to a *y* polarized mode in the situation where both modes are at equal power there is nothing to break the equivalence between the *x* and *y* directions.

It is also possible to achieve mode conversion by interaction between the fundamental and higher order modes of the same polarization. Figure 8(c) depicts the electrostrictive body force (green) and radiation pressure (blue) on the boundary of the waveguide for a combination of the fundamental and first order *x*-polarized optical modes. The SBS gain coefficient in this situation is 7.2×10^{3} $\mathrm{m}^{-1}\mathrm{W}^{-1}$ which results from an acoustic mode at frequency $\Omega/2\pi = 3.0$ GHz with wavevector $q = 4.9\times10^{6}$ m^{-1}.

Based on these optical forces a quasi-flexural acoustic mode is generated, shown in Fig. 8(d). Figure 9 depicts the coupling strength $\kappa_{\max}$ due to the interaction the *x*-polarized fundamental and first higher order modes for waveguides of differing width and height. We note that for widths below 490 nm the waveguide is not multi-moded over the whole of the wavelength range; we have therefore omitted this range of waveguide widths. Once again there is a significant increase of the coupling strength resulting from radiation pressure/boundary motion. In contrast to the cross polarized case considered in Fig. 7, the coupling strength is no longer

#221374 - $15.00 USD Received 26 Aug 2014; revised 17 Oct 2014; accepted 7 Nov 2014; published 14 Nov 2014

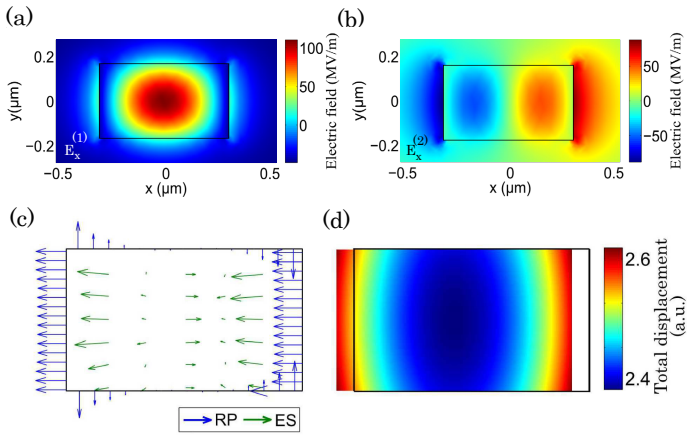

Fig. 8. a) Fundamental and b) first order *x*-polarized optical modes in a 550 nm by 350 nm silicon waveguide. Because one mode is even and the other is odd, an asymmetric acoustic mode is excited. c) Force distribution of radiation pressure (blue) and electrostriction body force (green) generated by applying fundamental and first higher order optical modes. d) corresponding magnitude of the total displacement of the acoustic mode generated by the forces. The strength of the acoustic oscillation is grossly exaggerated.

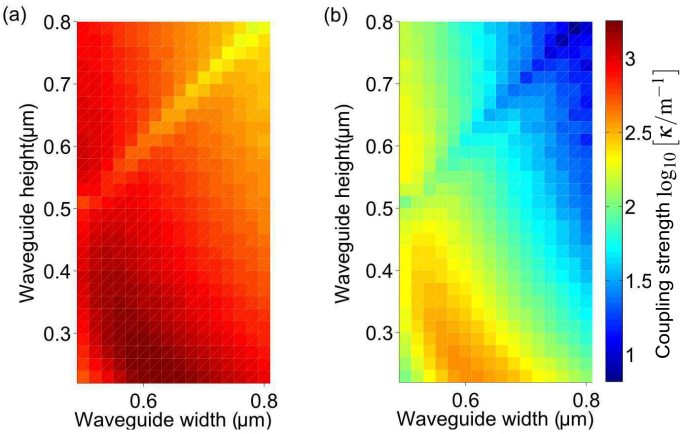

Fig. 9. Coupling strength $\kappa_{\max}$, expressed as $\log_{10}\left[\kappa/\mathrm{m}^{-1}\right]$ resulted from coupling between x-polarized fundamental and first higher order mode: a) by considering both electrostriction and radiation pressure (together with the photoelastic effect and waveguide boundary motion) and b) considering the electrostrictive effect and photoelasticity only.

symmetric with respect to waveguide geometry; this asymmetry arises because we have chosen the *x*-polarized mode for all waveguide geometries. A rapid change in the coupling strength along the line when the width and height are equal comes from an anti-crossing of the acoustic mode at this point.

5. Conclusion

We have investigated the effects of radiation pressure and waveguide boundary motion in Stimulated Brillouin Scattering (SBS)-driven mode conversion. We find that these effects play a significant role in the photonic transition achievable for high-contrast crystalline silicon nanowire

#221374 - $15.00 USD Received 26 Aug 2014; revised 17 Oct 2014; accepted 7 Nov 2014; published 14 Nov 2014

waveguides. For small waveguides the symmetry of the acoustic modes is important in determining which optical modes can be coupled using SBS.

Acknowledgments

This work was supported by the Australian Research Council (ARC) through its Discovery grant (DP130100832), Center of Excellence (CUDOS, CE110001018) and Laureate Fellowship (Prof. Eggleton, FL120100029) programs.

#221374 - $15.00 USD Received 26 Aug 2014; revised 17 Oct 2014; accepted 7 Nov 2014; published 14 Nov 2014

Optics Express

Title Details

Basic Description

Title	Optics Express
ISSN	1094-4087
Publisher	Optical Society of America
Country	United States
Status	Active
Start Year	1997
Frequency	Bi-weekly
Language of Text	Text in: English
Refereed	Yes
Abstracted / Indexed	Yes
Open Access	Yes http://www.opticsexpress.org
Serial Type	Journal
Content Type	Academic / Scholarly
Format	Online
Website	http://www.opticsinfobase.org/oe/journal/oe/about.cfm
Email	opex@osa.org
Description	Covers original research in optical science and technology.

Subject Classifications
Additional Title Details
Publisher & Ordering Details
Online Availability
Abstracting & Indexing
Other Availability
Demographics
Reviews

Save to List Email Download Print Corrections Expand All Collapse All